Plant Science 238 (2015) 13–25

Contents lists available at ScienceDirect

Plant Science

journal homepage: www.elsevier.com/locate/plantsci

Ups and downs in alfalfa: Proteomic and metabolic changes occurring in the growing stem

Bruno Printz[a,b], Gea Guerriero[a], Kjell Sergeant[a,*], Jenny Renaut[a], Stanley Lutts[b], Jean-Francois Hausman[a]

[a] Environmental Research and Innovation (ERIN) Department, Luxembourg Institute of Science and Technology (LIST), 5, Avenue des Hauts-Fourneaux, L-4362 Esch/Alzette, Luxembourg

[b] Groupe de Recherche en Physiologie végétale (GRPV), Earth and Life Institute Agronomy (ELI-A), Université catholique de Louvain, 5 (bte 7.07.13) Place Croix du Sud, B-1348 Louvain-la-Neuve, Belgium

ARTICLE INFO

Article history:
Received 24 March 2015
Accepted 16 May 2015
Available online 22 May 2015

Keywords:
Cell wall
Proteomics
DIGE
Stem
Cellulose synthase
Fibres

ABSTRACT

The expanding interest for using lignocellulosic biomass in industry spurred the study of the mechanisms underlying plant cell-wall synthesis. Efforts using genetic approaches allowed the disentanglement of major steps governing stem fibre synthesis. Nonetheless, little is known about the relations between the stem maturation and the evolution of its proteome. During *Medicago sativa* L. maturation, the different internodes grow asynchronously allowing the discrimination of various developmental stages on a same stem. In this study, the proteome of three selected regions of the stem of alfalfa (apical, intermediate and basal) was analyzed and combined with a compositional analysis of the different stem parts. Interestingly, the apical and the median regions share many similarities: high abundance of chloroplast- and mitochondrial-related proteins together with the accumulation of proteins acting in the early steps of fibre production. In the mature basal region, forisomes and stress-related proteins accumulate. The RT-qPCR assessment of the expression of genes coding for members of the cellulose synthase family likewise indicates that fibres and the machinery responsible for the deposition of secondary cell walls are predominantly formed in the apical section. Altogether, this study reflects the metabolic change from the fibre production in the upper stem regions to the acquisition of defence-related functions in the fibrous basal part.

1. Introduction

During development, plants are shaped through the activities of apical meristems, characterized by actively dividing cells, located in both roots and shoots. Under a tight hormonal control, procambial strands emerge from the shoot apex and differentiate into centripetal xylem, centrifugal phloem and an intervening layer of totipotent fascicular cambial cells: the vascular bundles [1–3]. In dicotyledonous plants, secondary development begins with the expansion of the interfascicular cambium which integrates with the fascicular cambium and mediates the production of parenchymal cells, conductive elements and lignified fibres to allow radial growth [1]. During this process of differentiation, the cells acquire specific functions and develop a novel architecture, which requires notable rearrangements in the wall components.

The plant cell wall, or "extracellular matrix", is a complex structure secreted by the cells and forms a restricted frame in which the plant protoplast develops. Growing cells initially develop a primary wall, a complex polysaccharidic network in which stiff cellulose microfibrils are embedded in a glue of hemicellulose and pectins [4]. Primary cell walls also contain 5–10% DW proteins. Once the cell ceases to grow, another layer, the secondary cell wall, is added between the plasma membrane and the rather flexible primary wall. This second layer typically consists of cellulose microfibrils having a higher degree of polymerization than in the primary wall, lignin, a complex polymer composed of phenylpropane units of very diverse structures and a limited amount of hemicelluloses, pectins and proteins. Secondary walls confer rigidity to the cells and can develop into specialized conductive cells involved in the formation of tracheary elements [4–6]. Besides their role in providing structural support to the cells, cell walls play active roles in the response to abiotic and biotic stress [4,7].

Alfalfa (*Medicago sativa* L.), a well-known forage crop cultivated since antiquity and commonly referred to as the "queen of

* Corresponding author. Tel.: +352 47 02 61 458; fax: +352 47 02 64.
E-mail address: kjell.sergeant@list.lu (K. Sergeant).

http://dx.doi.org/10.1016/j.plantsci.2015.05.014

forage" for the high nutritive value of its leaves, suffers from the poor digestibility of its stems [8–10]. Since cell-wall lignification is the major limitation in alfalfa digestibility, recent alfalfa crop improvement programmes have focussed on changes in lignin concentration and composition through modification of the expression of enzymes acting in the biosynthetic pathway of the two major monolignols, monomethoxylated guaiacyl (G) and dimethoxylated syringyl (S) [11,12]. In particular, down-regulation of C3H (coumarate 3-hydroxylase) and C4H (cinnamate 4-hydroxylase) acting in the early steps of monolignol biosynthesis resulted in increased stem digestibility [11].

Following alfalfa internode elongation, lignification occurs as part of a differentiation programme. Increasing stem maturity causes parallel changes in lignin composition (increase in the S:G ratio) and variation in polysaccharide concentrations, such as a decline in pectins, and an increase in cellulose and hemicellulose. This differential development observed along alfalfa stems can be used to discriminate, in the same stem, parts that differ in their differentiation process [13] and can thus be used to understand how stem and cell wall evolve/develop with time. Variations in stem composition can be determined with a panel of techniques, from the direct chemical characterization of the fibres [14] to the use of techniques based on molecular vibrations, such as near-infrared reflectance spectroscopy (NIRS) which allows the fast screening of large sets of samples [15].

Cell-wall synthesis is a complex process in which all cellular compartments are involved. The specific biosynthesis of monolignols starts with phenylalanine derived from the shikimate pathway occurring in plastids [16,17], which results in the formation of 3-*p*-hydroxyphenyl, guaiacyl and syringyl units and finally lignin, following the activities of numerous cytosolic enzymes, membrane-bound proteins and apoplast-located proteins [18]. Although cellulose synthesis depends essentially on large membrane-bound complexes—the cellulose synthase complexes (CSCs or rosette terminal complex) (that include a rosette-bound sucrose synthase) [19]—the biosynthesis of the main buildings blocks, the UDP-Glc units, derives from the activities of cytosolic UDP-Glc phosphorylases and proteins acting in the sugar and photosynthetic metabolism. Recent findings using confocal laser scanning microscopy techniques have highlighted the involvement of actin, Golgi vesicles and highly dynamic intracellular compartments referred to as SmaCCs/MASCs (small CESA compartments/microtubule-associated cellulose synthase compartments) as key partners for cellulose synthesis [20–22]. A role of these latter in the regulation of cellulose synthesis in response to environmental stimuli and in plant development programmes has been suggested [21,23].

Next to the classical genetic approach developed to understand cell-wall dynamics, proteomics has turned towards the development of complementary methods to analyze proteins from various cellular compartments (cytosolic, membranes) and plant apoplastic proteins were successfully isolated [24,25]. It remains nonetheless evident that each of these techniques provides a valuable tool to help unravelling how plants develop. Proteome analysis carried out on *Linum usitatissimum* L. in the region of the snap point, defined as the stem region in which the transition from cell elongation to secondary wall deposition occurs [26], revealed significant higher accumulation of enzymes acting in the primary metabolism, in cytoskeleton (tubulin, actin, myosin) and vesicular movement (dynamin-like proteins) in the fibre fraction; three processes that have been clearly demonstrated to participate in cellulose synthesis [21]. As such fibres also contain lignin [27], the accumulation of secreted peroxidases in this fibre fraction, in comparison to the non-fibre fraction, may be associated with the process of lignification [28].

Stems have thus been used to study vascular differentiation [29], however a proteome screening of different stem regions to analyze global developmental processes and more particularly fibre maturation is not documented. Here we describe a proteomic analysis of three selected regions of the alfalfa stem (apical–intermediate–basal) and assess the expression of the genes coding for members of the cellulose synthase family. This study is accompanied by structural analyses of the stem using optical microscopy, chemical and spectroscopic methods.

Altogether, this paper sheds light on the metabolic dynamism of the stem and highlights the existence of a switch from the production of fibres in the upper stem regions to the acquisition of defence functions in the mature, lower parts.

2. Materials and methods

2.1. Plant material

Alfalfa (*Medicago sativa* L. cv Giulia) seeds were inoculated with a peat-based inoculant (HiStick®, Becker Underwood) according to manufacturer's instructions and sown, three seeds *per* pot, in 1 L containers filled with soil (50% topsoil, 25% potting soil, 25% sand). Following germination, two of the three plants *per* container were selected. After 3 months of cultivation under greenhouse conditions (minimum temperature of 20 °C, supplemental lighting to reach a minimum of 13 h *per* day), the first growing shoots (consisting of 11 ± 1 internodes) of nodulated plants at the flowering stage were collected, leaves (including petioles and stipules) were separated with a blade and stems of about 50–60 cm long were divided into five parts for optical imaging, protein and gene expression analyses. For the analyses of the fibre content, shoots were divided into three parts (upper, middle and lower part). At the date of sampling, the plants developed a total of 2–3 growing shoots. Plant sections were numbered from the shoot tip to the base of the stem. Depending on the amount of plant material needed for the different analyses, a biological replicate consists of an individual first growing stem or a pool of first growing stems from different plants. Details about the sampling method and sample size are given in the following sections.

Plants were grown in two time-shifted batches (spring 2012 and spring 2013). The first batch, corresponding to 15 growing plants allowed analysing the soluble proteins and performing the optical imaging. A second batch, 30 plants, was dedicated to the quantification of the stem fibres and to the analysis of the genes coding for members of the cellulose synthase family.

Except for optical imaging and fibre analyses, stem parts were directly frozen into liquid nitrogen and stored at −80 °C prior to analysis.

2.2. Optical imaging

Internodes of each 1/5 stem segment were analyzed. Small sections, about 5 mm long from the middle of these internodes were fixed in 1.5 mL sodium phosphate buffer (0.2 M, pH 7.2) with glutaraldehyde (1%), paraformaldehyde (2%) and caffeine (1 g). Samples were placed under vacuum until fully impregnated. After impregnation samples were fixed (24 h, 4 °C) prior to being dehydrated in successive ethanol baths: (1) EtOH 70%, 30 min, (2) EtOH 70%, 60 min, (3) EtOH 95%, 30 min, (4) EtOH 95%, 60 min, (5) EtOH 100%, 30 min.

After dehydration, samples were impregnated (2 h) in a solution containing 50% (v/v) ethanol and 50% (v/v) glycol methacrylate resin with additional hardener I 1% (w/v) (Technovit® 7100). Finally, samples were saturated (24 h, 4 °C) in glycol methacrylate resin according to the manufacturer's instructions (Technovit®

7100, Heraeus Kulzer GmbH). After hardening, sections of 8 μm were sliced prior to staining with Fasga [30].

Stem growth and development were analyzed using the freeware ImageJ 1.45s. We assessed the development of the fascicular xylem along the stem by measuring, *per* internode, the maximal thickness of the xylem of five randomly selected vascular bundles. The values are expressed relatively to the average thickness of the xylem measured on the first internode (basal) (Fig. S1). A similar procedure was applied to assess the development of the vascular bundle including the sclerenchyma. The proportion of fascicular xylem per vascular bundle was determined by calculating the ratio between the maximal thickness of the xylem per vascular bundle and the maximal thickness of the corresponding vascular bundle (including sclerenchyma) based on five randomly selected vascular bundles per internode (Fig. S1).

2.3. Fibre analyses

Stems of similar height, homogeneous in their developmental stage (flowering) and consisting of 11 ± 1 internodes were pooled by 6, cut into pieces; the upper apical part (1/3), the intermediate part (2/3) and the basal part (3/3) to constitute 1 replicate each. In total, the fibre analyses were carried out on five replicates per stem part.

Fresh samples were dried at 70 °C for 3 days and crushed into powder with a Mortar Grinder RM 200 (Retsch). Near-infrared spectra of each sample were recorded and samples were further analyzed for dietary fibres using a gravimetric method.

2.3.1. Near-infrared spectroscopy

Near-infrared spectral data were collected using a near-infrared spectrometer (MPA, Brucker, Germany) equipped with an integrating sphere having a PbS detector (780–2780 nm) and the software OPUS 6.5. The milled samples were placed into quartz sample vials (flat bottom, 22 mm in diameter). The spectra were recorded at room temperature using the diffuse reflection method at wavelengths ranging from 800 to 2780 nm and with a resolution of 16 cm^{-1}. Each spectrum corresponds to a mean of 32 scans.

Spectra were further analyzed using the freeware R 2.15.2 with the additional packages "hyperSpec 0.98-20130301", "FactoMineR 1.25", "ChemometricsWithR 0.1.7", "signal 0.7-3" and "pcaMethods 1.50.0". Only the spectral range from 1350 to 2500 nm was used and spectral pre-treatments were applied. Spectral pre-treatments consisted of a baseline correction, a range scaling (each row is divided by the square root of the sum of its squared elements) followed by a spectral smoothing using a Savitzky–Golay filter (filter polynomial order: 2, filter length: 7). Spectral data were further mean-centred and Pareto scaling was applied.

A principal component analysis (PCA) using singular value decomposition (SVD) matrix factorization was carried out to check whether the NIRS spectra could qualitatively discriminated.

2.3.2. Fibre analysis

Fibre analysis was carried out using reagents as described by Van Soest *et al.* [14]. Following NIRS screening, stem fibres were sequentially digested using an Ankom^{2000} Fibre Analyzer in accordance with the recommendations for NDF (neutral detergent fibre), ADF (acid detergent fibre) and ADL (acid detergent lignin) analyses. In brief, 250–500 mg of the crushed dry material were placed in filter bags (F57 filter bag; ANKOM Technology Corp.), bags were heat sealed, weighed, placed in the bag suspender and inserted into the fibre analyser vessel prior to boiling in neutral detergent solutions with additional sodium sulphite and alpha amylase according to Ankom's instructions. For each run, three blank bags (empty) and three home-made internal standards (bags with approximately 500 mg dry alfalfa stem powder) were simultaneously digested to allow further blank bag correction and data normalization over the entire experiment. After extraction, bags were rinsed in acetone for 5 min, dried on a wire screen until acetone evaporation, completely dried in oven at 70 °C for 4 h and weighed. The same bags were then digested with acid detergent solution (ADF) following a similar procedure and weighed. Samples were finally digested for 3 h in 72% (w/w) sulphuric acid solution according to the Ankom's method for determining acid detergent lignin in beakers and finally weighed. Calculations were performed as follows:

%Fibre (NDF or ADF or ADL) = 100 × (dried weight of bag with fibre after extraction process–(bag tare weight × blank bag correction))/DW of the initial sample

The proportion of hemicellulose and cellulose were estimated, respectively, by calculating the difference between the percentage of neutral detergent fibre (%NDF) and the percentage of acid detergent fibre (%ADF) and by calculating the difference between the percentage of acid detergent fibre (%ADF) and the percentage of acid detergent lignin (%ADL). Starch and soluble pectic substances were estimated by the formula (1−%NDF) and the proportion of lignin was estimated by the percentage of ADL (%ADL).

2.4. Protein analyses

2.4.1. Plant sampling

For protein extraction, the first growing stem (11 ± 1 internodes) from five individual plants homogeneous in their developmental stage (flowering) was divided into five parts. Each resulting plant part was annotated from the apical (1/5) to the basal (5/5) end. Only parts 1/5 (apical), 3/5 (intermediate) and 5/5 (basal) were selected for proteomic characterization. One proteomic replicate consisted of a single stem section from one individual plant. Protein extraction and quantification were performed on the five replicates and four were randomly selected for DIGE analysis, resulting in a total of 12 samples (3 stem parts × 4 plants).

2.4.2. Protein extraction

Frozen samples were ground to powder in a mortar precooled with liquid nitrogen and proteins were extracted using a TCA/phenol-SDS protein extraction method as follows.

The crushed stem from each replicate was transferred to 2 mL microtubes and re-suspended in 1 mL ice-cold TCA (20%, w/v) in acetone with 0.1% (w/v) DTT. Proteins were precipitated for 60 min at −20 °C, samples were centrifuged (10,000 × *g*, 4 °C, 5 min) and the supernatant was discarded. After precipitation, the pellets were washed in 1.5 mL of ice-cold acetone and centrifuged again (10,000 × *g*, 4 °C, 5 min). This washing step was repeated twice and the pellets were subsequently dried under low pressure.

Pellets were re-suspended in 800 μL of UltraPure™ Buffer-Saturated Phenol (Invitrogen) and 800 μL of SDS buffer (30%, w/v) sucrose, 2% (w/v) SDS, 0.1 M Tris–HCl, pH 8.0, 5% (v/v) 2-mercaptoethanol, mixed in an Eppendorf Thermomixer (1400 rpm, 20 °C, 20 min) and subsequently centrifuged (11,000 × *g*, 20 °C, 5 min) to allow the separation of the phenolic and the SDS–buffer phases.

For each sample, two volumes of 300 μL of the phenolic phase, at top of the tubes, were collected in two separated 2 mL microtubes. In each tube, proteins were precipitated by adding 1.5 mL of ice-cold 0.1 M ammonium acetate in methanol and kept overnight at −20 °C. Samples were centrifuged (10,000 × *g*, 5 °C, 5 min) and the pellets were washed twice with 0.1 M ammonium acetate in methanol. Samples were finally washed two more times in ice-cold acetone/water (80/20, v/v) and re-suspended in 50 μL of labelling buffer (7 M urea, 2 M thiourea, 30 mM Tris, 2%, w/v, CHAPS). Samples were shaken in an Eppendorf Thermomixer (700 rpm, 20 °C, 60 min), centrifuged (14,000 × *g*, 30 s) to remove insoluble material and both extracts from the same sample were re-pooled. Prior to

quantification, the pH of the samples was adjusted to 8.5 using 1 M HCl. Protein quantification was carried out with Bradford protein assay using BSA as standard [31].

2.4.3. Protein labelling

Proteins, 50 μg of each sample, were labelled with 400 pmol of dyes LUMIPROBE LLC 25 nM (Interchim®). Cy2 was used for the internal standard, a sample made of the same amount of proteins from all samples, and Cy3 or Cy5 were used to label the different samples. Labelling was carried out in the dark at 4 °C. After 30 min incubation, the reaction was quenched by the addition of 1 μL 10 mM lysine and a further 10 min incubation in the dark at 4 °C. Samples were pooled by 2, an equal volume of internal standard was added and the volume was adjusted to 450 μL with lysis buffer (7 M urea, 2 M thiourea, 0.5%, w/v, CHAPS). Finally, 2.7 μL Destreak Reagent (GE-Healthcare) and 1.5% (v/v) Ampholyte (Bio-Rad) (pH 4–7) were added and samples were loaded onto Immobiline™ DryStrip (3–7 NL, 24 cm) for overnight rehydration.

2.4.4. Protein migration and analysis

Isoelectric focusing (IEF) was carried out at room temperature in a five-step programme: (1) constant 100 V for 3 h, (2) 4 h linear gradient from 100 to 1000 V, (3) constant 1000 V for 5 h, (4) 6 h linear gradient from 1000 to 10,000 V, (5) constant 10,000 V voltage until reaching a total of 90,000 V h. During IEF, the current was limited to 75 μA per strip.

Prior to the second dimension, strips were equilibrated 15 min in equilibration buffer (Serva Electrophoresis GmbH, Heidelberg) complemented with 6 M urea and 1%, w/v, DTT and further 15 min in equilibration buffer (Serva Electrophoresis GmbH) complemented with 6 M urea and 2.5%, w/v, IAA. Strips were then loaded on 2D HPE™ Large Gels NF 12.5% (Serva Electrophoresis GmbH) and electrophoresis was carried out using an HPE™ Tower System according to manufacturer's instructions. After the front reached the bottom of the gel, the proteins were fixed in a solution containing 15% (v/v) ethanol complemented with 1% (m/v) of citric acid at least 2 h and rinsed with MQ water. Gels were subsequently scanned using a Typhoon FLA 9500 scanner (GE-Healthcare), and quantitative analysis was carried out using the DeCyder software (v7.0, GE-Healthcare). Spot comparison was performed by calculating the ratio r between the average intensity of a spot in the different stem parts. In case this ratio was superior to 1, we reported a fold-change equal to r. In case r was inferior to 1, we reported a fold-change equal to $-1/r$. An absolute fold-change superior to 1.5 was considered to be significant (Student's t-test, p-value ≤ 0.05). Picking, digestion, MALDI spotting and MS analyses were carried out as described by Printz *et al.* [32]. MS and MS/MS spectra were submitted for NCBInr database-dependent identification using the taxonomy *viridiplantae* (http://www.ncbi.nlm.nih.gov) downloaded on January 18, 2013, and containing 22,586,145 sequences on an in-house MASCOT server (Matrix Science, www.matrixscience.com). A second search was carried out against an EST eudicots database downloaded on July 17, 2012, and containing 14,452,337 sequences. Protein identifications, including MS/MS and spot data, are available in Table S1a, 1ba, 1b and 1c.

2.5. Gene expression analyses

Twenty-four first growing stems (11 ± 1 internodes) homogeneous in their developmental stage (flowering) were divided into five parts. Each resulting plant segment was annotated from the apex (1/5) to the base (5/5) and pooled by 6 to constitute 4 replicates per stem part.

Since the alfalfa genome is currently not available, the sequences retrieved from the available genome of barrel medic (*Medicago truncatula*) were used to design primers. The genome of the closely related barrel medic was indeed reported to be suitable for molecular analyses on alfalfa [13]. The sequenced genome of *M. truncatula* was therefore mined to determine the number of putative cellulose synthase genes (*CesA*s), by blasting the full-length sequences reported in *Arabidopsis thaliana* and *Populus trichocarpa* [33]. Nine genes were identified which code for proteins belonging to both the primary and secondary cell-wall clade. Primers for qPCR analysis were subsequently designed on the *M. truncatula CesA*s as reported below, in order to amplify and study the orthologs from alfalfa.

2.5.1. RNA extraction and cDNA synthesis

Sampled tissues were initially ground in liquid nitrogen using a mortar and a pestle, then pulverized using a TissueLyser and 5 mm autoclaved stainless steel beads. Special care was taken to keep the samples frozen and prevent thawing.

Total RNA was extracted using the RNeasy Plant Mini Kit coupled to the on-column DNase treatment (Qiagen) for removal of genomic DNA. The integrity of the extracted RNA was checked using an Agilent Bioanalyzer (RINs were all >8) and the purity/concentration measured with a NanoDrop ND-1000 spectrophotometer. Subsequently 1 μg of DNase-treated RNA was retro-transcribed using the Superscript II cDNA Synthesis Kit (Invitrogen), according to the manufacturer's instructions.

2.5.2. Real-time PCR

For real-time PCR analysis, 10 ng of cDNA were used as template. The cDNA was amplified using the MESA GREEN qPCR MasterMix Plus Low ROX (Eurogentec) on a ViiA 7 Real-Time PCR System (Applied Biosystems).

The reactions were performed in triplicates and repeated on four biological replicates. The PCR conditions consisted of an initial denaturation at 95 °C for 10 min, followed by 45 cycles of denaturation at 95 °C for 15 s, annealing/extension at 60 °C for 60 s.

A dissociation kinetics analysis was performed at the end of the experiment to check the specificity of the annealing. The amplicons were all verified by sequencing.

The primers used to perform real-time PCR analyses are listed in Guerriero et al. [33].

The stability of 10 candidate reference genes, namely actin, tubulin, ubiquitin-conjugating protein 13 (UBC13), cyclophilin, elongation initiation factor 4A (eif4A), elongation initiation factor 5A (eif5A), translation initiation factor IIA (TFIIA), glyceraldehyde-3P dehydrogenase (GAPDH), actin-depolymerizing protein (ADF1), poly(A) binding protein 4 (PAB4) was evaluated using geNorm^{PLUS} [34]. The candidate reference gene primers for actin, tubulin and GAPDH were designed on the sequences from *M. truncatula* (accession numbers XM_003621971, XM_003603622, XM_003595990, respectively). The other primers were designed on the sequences reported in Yang et al. [35]. Following assessment of the Ct values, three independent biological replicates were retained for statistical analysis.

The results were analyzed using the software qBase^{PLUS} [36] and normalized using the six most stable genes belonging to different functional classes (ADF1, cyclophilin, PAB4, TFIIA, eif4A, eif5A). The expression levels of the genes detected in the different stem regions analyzed are here expressed as relative normalized expression. A one-way ANOVA (with Tukey's HSD post hoc test) was performed on the $\log_2$-transformed values using IBM SPSS Statistics (version 19), after having checked the normal distribution of the data with a with a Kolmogorov–Smirnov test. Hierarchical clustering was generated with Cluster 3.0 [37] and visualized with Java TreeView [38], available at http://jtreeview.sourceforge.net/

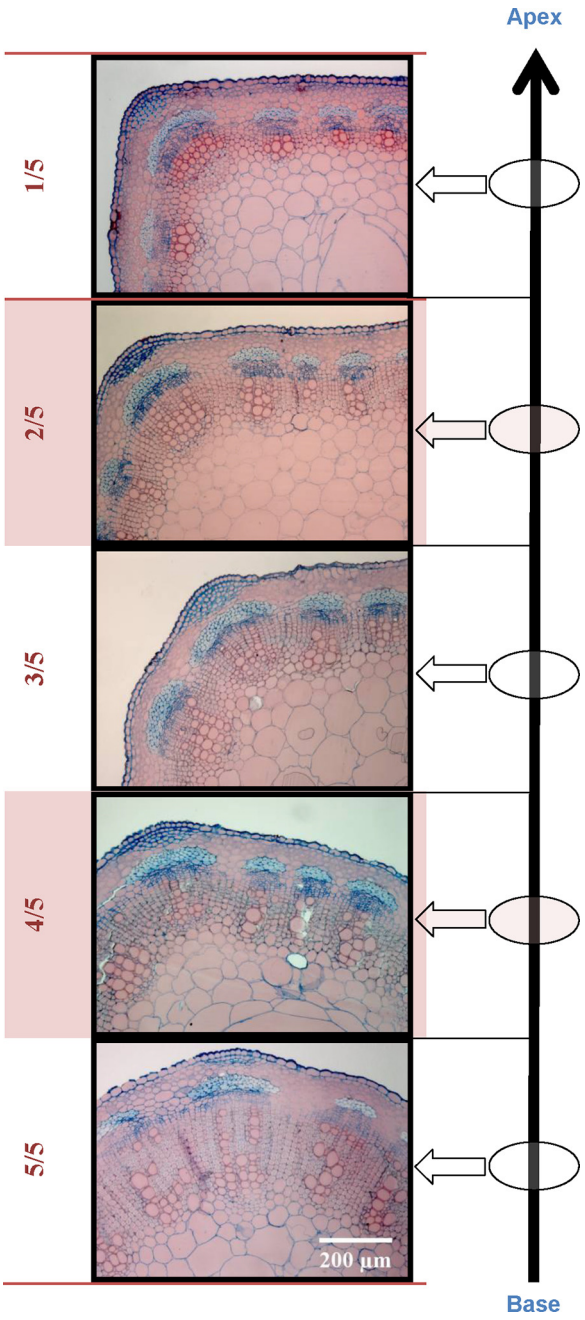

Fig. 1. Optical imaging of alfalfa stem regions stained with Fasga coloration (thickness: 8 µm). Sections are organized from the apex (1/5) to the most basal region of the stem (5/5).

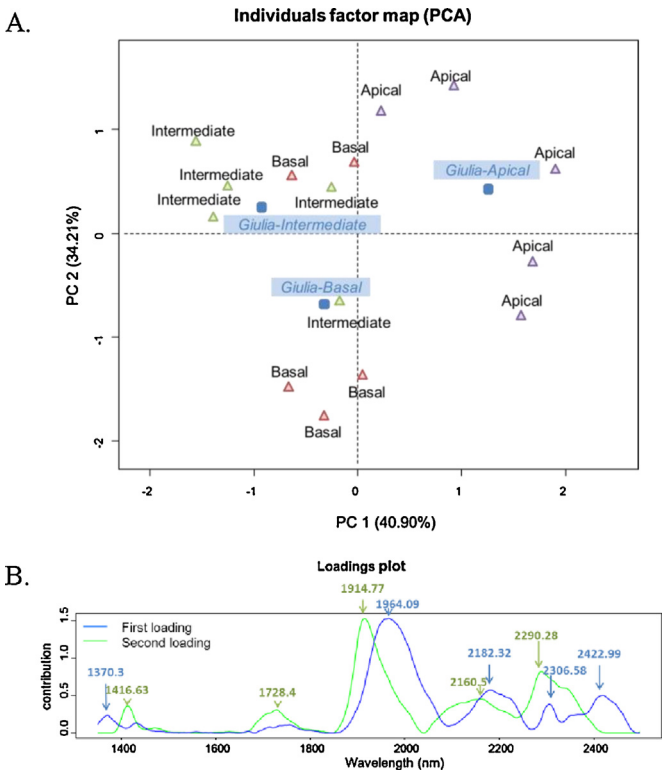

Fig. 2. NIRS analysis of the three stem regions (apical–intermediate–basal). (A) Principal component analysis of the pre-treated NIRS data. Represented are the two main axes accounting for 75.11% of the total variability of the cloud of points. Note that the first dimension allows for discrimination of the apical part from the lower stem parts and that the second dimension reflects the biological variability between samples. Blue boxes represent the barycentre of the five individual measurements from a same stem region. (B) Loading plot of the two first PCA loadings.

3. Results

In this study, the stem of alfalfa was divided into fifth and annotated from the apex (1/5) to the base (5/5). This paper is mainly focused on the three stem segments: (a) apical (1/5), (b) intermediate (3/5) and (c) basal (5/5).

3.1. Histological imaging and fibre analysis

With optical imaging, a gradual increase in stem secondary growth was observed from the apex to the base of the stem (Figs. 1 and S1). In the most apical fifth (1/5), the vascular bundles composed of primary xylem, primary phloem and cambium are separated by thin-walled parenchymal cells. Secondary phloem and xylem begin to develop. From the next region down (2/5), the interfascicular cambium differentiates to form a continuous ring with the fascicular cambium (Fig. 1). Interfascicular parenchyma undergoes primary wall thickening. Gradually, the cambial ring produces lignocellulosic centripetal xylem and cellulosic centrifugal phloem (Fig. 1). From the fourth fifth, fascicular and interfascicular xylem elements form a homogenous structure. The fascicular xylem and the vascular bundle follow a regular linear thickening from the apex to the base of the stem (Fig. S1A–C). The proportion of fascicular xylem per vascular bundle increases from the apex (1/5) to the second fifth of the stem but tends to stabilize in the most basal regions (5/5) (Fig. S1D).

To assess the composition of the stem at the structural level, near-infrared (NIR) absorbance spectra of dry powder resulting from the grinding of the different stem parts were recorded. PCA analysis revealed that the first axis of the PCA, accounting for 40.90% of the total variability of the cloud of points, separates the apical samples from intermediate and basal samples (Fig. 2). Since NIR spectroscopy relies on molecular overtones and the combined vibrations of the chemical bonds C—H, O—H and N—H [39], the segregation of the samples from the apical region indicates that this region has a distinct molecular composition compared with the lower parts. From the loading plot (Fig. 2B), five absorbance regions having a maximal height at 1370.3, 1964.09, 2182.32, 2306.58 and 2422.99 nm can be distinguished, indicating variation in the abundance of the functional groups CH_3, RCO_2R, $CONH_2$, RNH_2 and C—C in the apical part in comparison with the two lowest regions [40]. The second axis of the PCA that accounts for 34.21% of the total variability emphasizes a high heterogeneity existing between the

different replicates and is attributed to absorbance regions having a maximum at 1416.63, 1728.4, 1914.77, 2160.5 and 2290.28 nm.

Since the NIR spectroscopy analysis indicates changes in molecular composition with increasing maturity, we performed an Ankom Fibre gravimetric analysis to estimate the proportion of the main structural compounds of the stem, soluble compounds/starch/pectins (1−%NDF), hemicellulose (%NDF−%ADF), cellulose (%ADF−%ADL) and lignin (%ADL) in each stem part (Fig. S2). Confirming the NIR-obtained segregation of the samples from the apical extremity on the first axis of the PCA (Fig. 2), the apical extremity contains significantly less of the structural polymers cellulose and lignin, but not hemicellulose, than the two lower stem parts. In contrast, the composition of the intermediate and lower stem parts does not significantly differ (Fig. S2). These lower proportions of cellulose and lignin are compensated by a significant higher proportion of hydrosoluble compounds/starch/pectins in the apical part in comparison to the two other stem sections (Fig. S2).

3.2. Proteome analyses using 2D difference in-gel electrophoresis

The development of alfalfa stem was assessed by profiling the proteome of three stem parts from the elongating apical extremity to the thick-walled basal region. The intermediate sample was analyzed in order to aid in the disentanglement of the metabolic switch occurring between primary and secondary growth. Among the 3000 spots detected on each gel, 60 proteins significantly differ in abundance between the apical and the basal part (p-value t-test < 0.05, absolute fold-change > 1.5), 8 between the apical and the intermediate part, and 36 between the intermediated and basal region (Table S2). Contrary to the gravimetric fibre analysis, the proteomic data indicate a high similarity between the young, apical and the intermediate region, rather than between the intermediate and the mature, basal segment. In fact an important metabolic switch occurs slightly below the intermediate stem region (Table S2).

Among the biological processes affected by the set of proteins which significantly differ between the different stem regions, most changes in abundance are observed for proteins involved in biotic and abiotic stresses and in controlling cellular processes (Fig. 3A). When sorted according to the cellular compartment in which the differentially accumulated proteins occur, our study highlights that the chloroplast machinery and the apoplast are major sites of modifications (Fig. 3B).

Stems are commonly described as biological structures involved in the transport of water, nutrients and assimilates via the two typical paths formed by the xylem vessels (transport from root to shoot/leaves) and the sieve tube elements of the phloem (transport from source to sink). Although leaves are the most photosynthetically active organ in plants, stems also perform photosynthesis [41,42]. During leaf maturation, the metabolism of leaves switches from sink to source, once photosynthetic activity is fully established [43]. Here, we gathered cues supporting that the photosynthetic metabolism undergoes clear maturation in stems.

3.3. CesAs expression

In plant, the machinery of cellulose synthesis involves cellulose-synthase rosettes, functional cellulose-synthesizing complexes exhibiting a multicatalytic glycosyltransferase activity [44,45]. Depending on the type of growing wall, the formation of the rosette involves proteins encoded by different *CesA* genes [46–48]. However, recent studies indicated that mixed primary and secondary CESA complexes retain functionality [49,50], therefore a certain flexibility/promiscuity in terms of interacting partners exists in plant CESAs at certain stages. To check for differences in the expression of genes involved in the formation of cellulose-synthase rosettes between the stems parts, we identified the genes coding for cellulose synthases (*CesA*s) in *M. sativa* and followed their expression along the stem (Fig. 4). Although significant differences in gene expression were recorded for *CesA* genes putatively involved in primary (*CesA1*, *CesA6-C*) and secondary wall deposition (*CesA4*, *CesA7-A*, *CesA8*), the most remarkable variations in *CesA* gene expression are observed for the genes related to secondary wall biogenesis (Table 1). Relative to the basal segment, the expression of *CesA7-A* and *CesA8* shows a 12.12-fold to 18.33-fold increase in the upper stem regions.

Table 1
Average expression level of the cellulose synthase gene expressed relatively to the expression measured in the basal region (5/5).

	Gene	4/5	3/5	2/5	1/5
Primary wall	*CesA1*	0.80	1.00	1.23	1.19
	CesA3	0.93	1.10	1.08	0.97
	CesA6-B	1.10	1.19	1.09	0.94
	CesA6-C	0.99	1.62	2.79	2.65
	CesA6-F	1.16	1.46	1.67	1.55
Secondary wall	*CesA4*	0.89	1.82	3.96	5.42
	CesA7-A	1.46	3.73	12.40	12.12
	CesA7-B	1.09	1.53	2.27	3.45
	CesA8	1.39	4.84	18.33	16.69

4. Discussion

4.1. The machinery of protein synthesis

The current proteomic dataset sheds light on the complexity of the regulation of protein synthesis and degradation along the stem and among the different cellular compartments. According to the evolution of the spot volumes, two sets of proteins can be distinguished (Fig. 5A and B). The first regroups the proteins in the spots 321, 512, 701, 1138, 1392 and 2971 (Fig. 5A) that are of higher abundance in the upper regions, the second clusters spots 205, 693, 1924, 2385 and 2546 (Fig. 5B) and contains proteins that accumulated more in the fibrous basal region.

The young apical stem segment accumulates proteins playing a role in the broad process of chloroplast protein synthesis, spanning from the control of RNA stability to the acquisition of the final structure of the protein (CSP41-b (spot 1392), EF-Tu (spot 1138), EF-G (spot 321), Cpn60 (spot 701)). One HSP 70 (spot 512), involved in protein folding and refolding, but without evidence of chloroplast location, also follows a similar accumulation as Cpn60. Globally, this indicates that this region is a site of high chloroplastic protein metabolism. In contrast, the second cluster group proteins that accumulate with increasing stem maturity (Fig. 5B), which are involved in cytosolic protein biosynthesis (eIF-5a (spot 2385)), maturation (endoplasmic protein disulfide isomerase (spot 693)), turnover (HSP90 (spot 205)), and protease regulation (proteasome subunit alpha type-2-A-like (spot 1924)). We noticed in particular that one stalk ribosomal proteins P3-like (spot 2546) is of higher abundance in the basal region. In *Nicotiana benthamiana*, silencing of a homolog of this protein resulted in reduced *Potato Virus A* infection. This reduction is attributed to a limited translation and indicates that the presence of the stalk is important in the regulation of the translation process [51]. Globally, and although the protein content measured in the most mature region was significantly lower than in the apical region (Table S3), the fibrous base of the stem remains a site of active protein metabolism.

4.2. Chloroplastic activity of alfalfa growing stems

The synthesis of the cell-wall components starts with the production of activated nucleotide sugars (for cellulose,

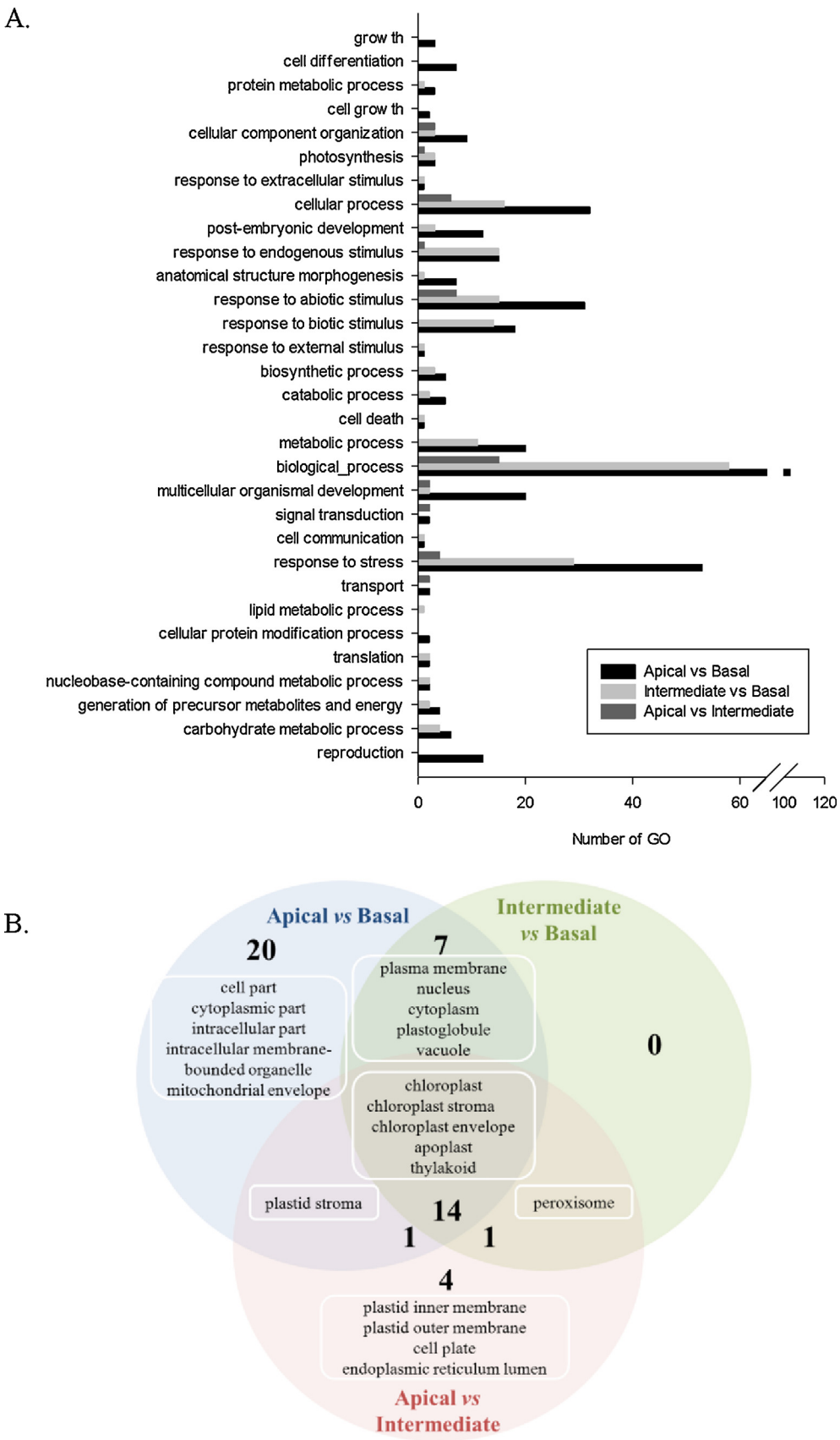

Fig. 3. Clustering and Venn diagram obtained from the differentially accumulated proteins. (A) Clustering of the differentially expressed proteins according to the biological process in which they are involved. Number of GO corresponds to the occurrences in the classification according to gene ontology. (B) Venn diagram of the cellular compartments in which the differentially expressed proteins are localized. Gene ontology annotation and clustering were carried out using the online tools Goanna, GOSlimViewer and GOSlimAuto available at the Agbase website (http://agbase.msstate.edu).

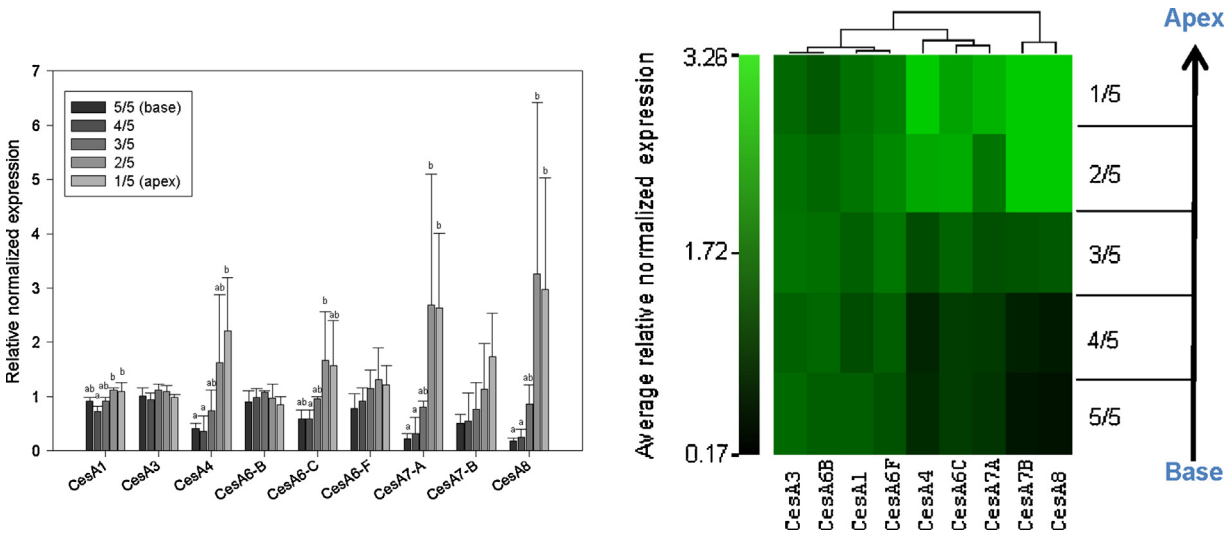

Fig. 4. Expression profile of the different cellulose synthase genes along the stem of alfalfa plants (cv. Giulia) and associated hierarchical clustering. Stems were cut in fifths and annotated from the apex (1/5) to the most basal segment (5/5). Error bars represent standard deviation. Multiple comparison of means was carried out using three biological replicates per stem part and determined following Tukey's HSD test. Each letter corresponds to a group that is significantly different from the others (p-value < 0.05). Note the significant increase in expression of all genes involved in secondary cellulose deposition in the upper stem regions (*CesA4*, *CesA7-A*, *CesA8*).

hemicellulose and pectin production) and early shikimate precursors (for lignin synthesis). In plants, the use of carbon directly derived from photosynthesis or remobilized from the non-reducing sugar sucrose represents the major source of carbon for the generation of nucleotide sugars [52]. Similarly, a close connection exists between photosynthetic activity and lignin synthesis [53].

Similar to growing leaves, the apical extremity of the stem undergoes specific maturation to develop the chloroplast machinery. Although the process of thylakoid biogenesis remains unclear, a dynamic system of vesicle transport and the assistance of several factors appear to be essential for the biogenesis of thylakoids in mature chloroplasts [54,55]. In *A. thaliana*, deficiency in one of these factors (Thf1) resulted in accumulation of membrane vesicles in chloroplasts without forming thylakoids. TEM analysis of transgenic lines, in which Thf1 cDNA is introduced in antisense orientation, confirmed that the presence of Thf1, which accumulates in the apical part (spot 1840, Fig. 5C), governs normal thylakoid organization [54].

A similar pattern of accumulation is observed for spot 1163 identified as a glutamate-semialdehyde (GSA) aminomutase (Fig. 5C). The first part of the chlorophyll biogenesis is the conversion of glutamic acid to 5-aminolevulinic acid (ALA) in a three-step pathway involving the activation and reduction of a glutamic acid and a final conversion to ALA catalyzed by a GSA aminomutase [56]. The formation of the precursor ALA has been proposed as the rate-limiting step in chlorophyll synthesis [57]. Although proteomics does not provide information on protein activity, the higher abundance of GSA aminomutase (spot 1163) indicates that porphyrin metabolism and the acquisition of thylakoid organization may follow a similar regulation (Fig. 5C). In the apical region, we noticed, in parallel, an accumulation of a 6-phosphogluconate dehydrogenase (spot 943) which catalyses the decarboxylating reduction of 6-phosphogluconate into ribulose 5-phosphate, the last step of the oxidative part of the pentose phosphate pathway (Fig. 5C) and also involved in generating NAPDH from $NADP^+$.

Proteins located in the thylakoid membrane and directly involved in photophosphorylation reach a maximum abundance in the medium and apical regions, suggesting that chloroplastic activity of the stem is maintained below the medium part of the stem (Fig. 5D). One light harvesting chlorophyll-a/b binding protein Lhcb I (spot 1971) together with a photosystem I subunit VII (spot 2902) are significantly more abundant in the apical and the intermediate parts in comparison to the basal stem region (Fig. 5D). Since these proteins are part of the photosystem supercomplexes and have been demonstrated to play a role in their activity and in the transfer of excitation energy [58–60], their increased abundance in the apical extremity of the stem may be associated with higher resonance energetic transfer to the reaction centre of the photosystem, leading consequently to a higher flux of electron through the thylakoid membrane.

Consistent with this assumption, a higher abundance of ferredoxin-$NADP^+$ reductase involved in the production of the reducing agent NAPDH (spots 1508 and 1519) [61] and chloroplast ATPase subunits (spots 189, 803 and 884) is observed in the two upper stem regions in comparison to the basal one (Fig. 5D).

During photophosphorylation, bicarbonate ions are pumped in the thylakoid by using the proton gradient and are converted into CO_2 by carbonic anhydrases [62]. Photophosphorylation can thus be seen as a global process that delivers a coordinated supply of ATP, NAPDH and CO_2 to the Calvin cycle [63] (Fig. 6). As shown by the higher abundance of proteins acting in C-fixation, namely cytosolic and chloroplastic carbonic anhydrases (spots 1185, 1832, 1965, 1977 and 1993) (Fig. 5E), fragments or subunits of the ribulose-1,5-bisphosphate carboxylase/oxygenase (spots 770, 797, 810,846, 851, 859, 862, 872, 877, 879, 881, 904 and 2692), chloroplast fructose bisphosphate aldolase (spots 1299, 1312 and 1316) (Fig. 5F) and RubisCO activase (spot 1256) in the 2 most apical segments, the Calvin cycle appears to be the main acceptor of the products of photophosphorylation occurring at this site (Fig. 5F). Interestingly, one chloroplastic 2-cys peroxiredoxin BAS1 (spot 2090) known to protect the photosynthetic apparatus, increases in abundance in the intermediary region relatively to the basal extremity [63] (Table S2 and Fig. 5F).

The interaction between the leaf and the non-foliar photosynthesis is complex and was mostly studied for plants living in deserts and Mediterranean habitats. In plants, the stem net photosynthetic rate can represent up to 60% of the leaf net photosynthetic rate and contributes positively to the carbon gain of the plant [64,65]. Age-dependency of stem-internal CO_2 refixation was however reported in woody stems which develop lignified tissues and a protective bark layer [64]. In our study, the differential accumulation of proteins involved in chloroplast activity highlights the metabolic

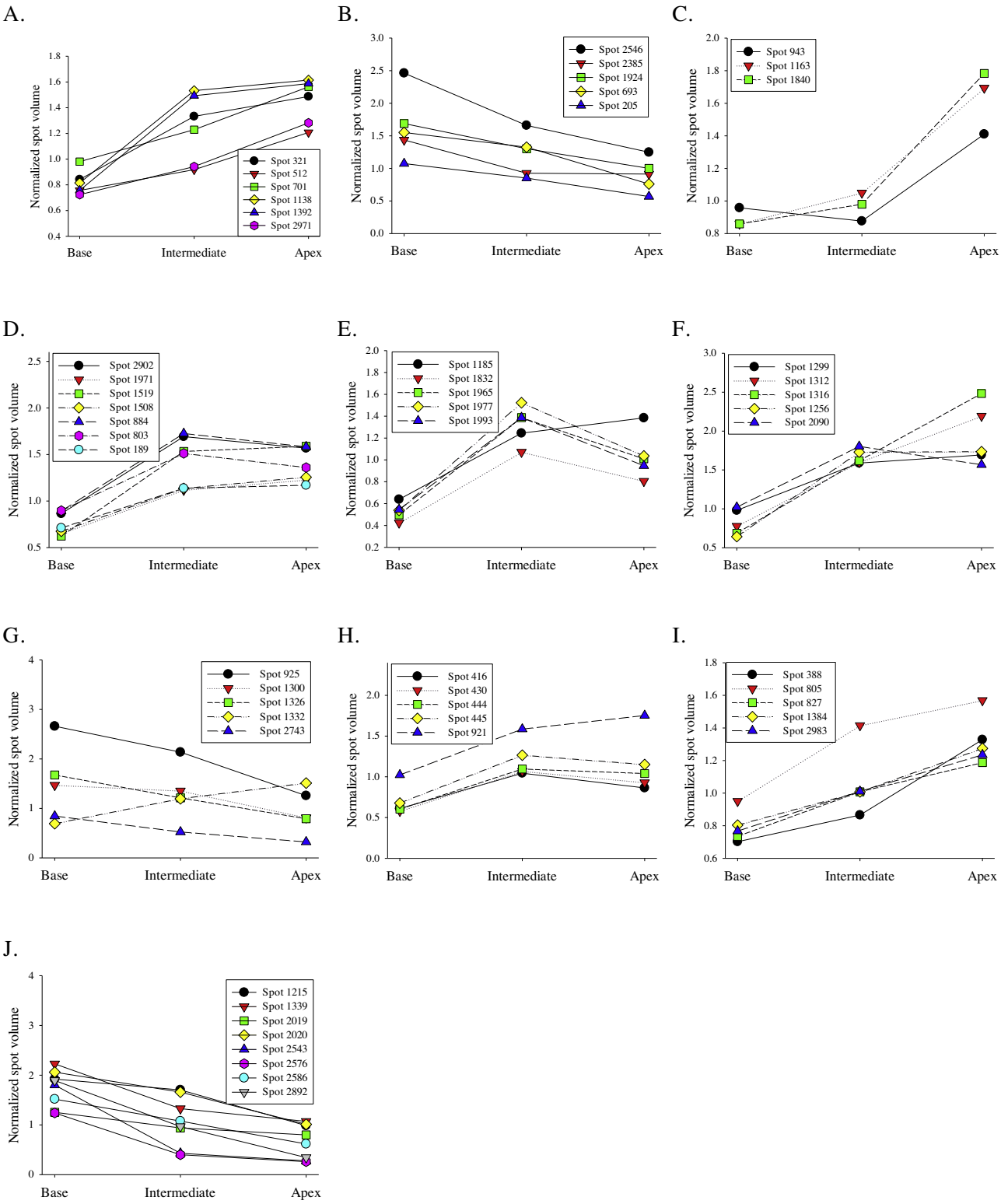

Fig. 5. Profile of the abundance of spots (expressed as normalized volume) in the different parts (base, intermediate, apex) of the alfalfa stem. (A, B) Protein biogenesis and catalysis; (C–F) chloroplastic activity; (G) sucrose biosynthetic pathway; (H) Shikimate precursors; (I) mitochondrial respiration; (J) redox regulation and stress-related proteins.

switch that occurs between the two youngest stem regions and the woody basal segment (Fig. 6). In particular, this change is accompanied by the stabilization of the proportions of fascicular xylem per vascular bundle (Fig. S1D) at the microscopic scale, by the stabilization of the fibre composition as revealed by the clustering of the medial and basal stem regions (Fig. 2) and by the absence of significant difference in the proportions of fibre down from the intermediate stem region (Fig. S2).

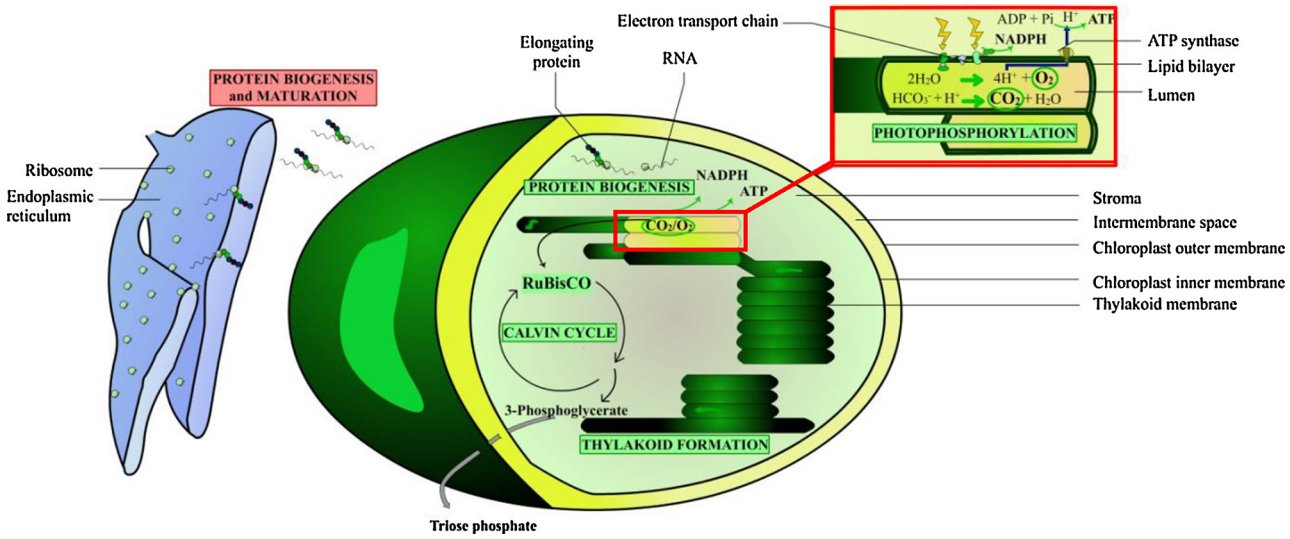

Fig. 6. Evolution of the chloroplast proteome in the apical (1/5) vs basal (5/5) stem regions of alfalfa. Green and red-filled boxes indicate, respectively, biological routes in which proteins are of higher and lower abundance in the apex.

4.3. Partitioning of the carbon fixed during the Calvin cycle

4.3.1. Sucrose biosynthetic pathway and cellulose synthesis

Assuming a higher photosynthetic activity in the apical and intermediate regions in comparison with the basal one would consequently increase the availability of triose-phosphates in the cytosol of the two youngest stem parts. Cytosolic fructose-1,6-bisphosphatase (cFBPase) (spot 1332) accumulates in the upper parts of the stems, particularly in the apex (Fig. 5G). In rice (*Oryza sativa*) and *A. thaliana*, decreased expression of cFBPase resulted in decreased sucrose level and photosynthetic rate in day conditions [66,67]. In transgenic *A. thaliana* plants, overexpression of cFBPase together with a chloroplastic envelope phosphate/phosphate translocator (TPT) resulted in enhanced photosynthetic activity and increased levels of soluble sugar and starch [68]. Based on these observations and since cFBPase catalyses the unidirectional conversion of fructose-1,6-bisphosphate to fructose 6-phosphate in an early step of sucrose synthesis, the higher accumulation of cFBPase in the apical extremity of the stem suggests a higher flux of carbohydrates to the sucrose synthesis pathway in the upper stem regions. Since the production of UDP-glucose is depending on this route, the increase in cFBPase may drive a higher flux of this precursor in the intermediate and apical stem regions. This hypothesis is consistent with the enrichment of cellulose in the cell wall observed between the apical and the intermediate stem segment (Fig. S2).

The higher expression of genes coding for the production of cellulose synthase subunits involved in secondary cell-wall synthesis may indicate that the main site of secondary wall CSC formation is located in the upper regions of the stem (Fig. 4). Nonetheless, since microscopic imaging indicates a constant increase in secondary development with stem maturation (from the apex to the base; Figs. 1 and S1A and B), the machinery of cellulose synthesis in secondary walls may stay active all along the stem.

A higher accumulation of clathrin light chain (CLC) proteins (spot 925, Fig. 5G) was further observed in the intermediate and basal regions of the stem. Besides controlling the establishment of auxin transporters, mediating plant hypersensitive response, participating in cell plate formation and modulating membrane turnover [69], clathrin-mediated endocytosis is used by plants to regulate the abundance of active cellulose synthase complexes CSCs at the plasma membrane [70]. Also established is the role of cortical microtubules and actin in the delivery of CSCs to the plasma membrane [20,21]. Although no cytoskeletal protein was found differentially accumulated in this study, one prefoldin subunit (spot 2743), shown to be able to form stable binary complexes with nascent unfolded actin and tubulin [71], accumulated in the basal region in comparison with the two upper stem segments.

Simultaneously, we noticed a significant lower abundance of glyceraldehyde-3-phosphate dehydrogenase (GAPDH) (spots 1300 and 1326) involved in producing 1,3-bisphosphoglycerate in glycolysis in the upper stem parts relatively to the lower region (Fig. 5G). In the apical extremity, the decrease in GAPDH may further limit the production of 3-phosphoglycerate (3-PGA) through glycolysis and favour its production through the Calvin cycle. In contrast, the generation of 3PGA through glucose catabolism appears enhanced in the lower region.

4.3.2. Shikimate pathway and phenylpropanoid metabolism

The entry point into the shikimate pathway is the production of shikimate from erythrose-4-phosphate and phosphoenolpyruvate by the 3-deoxy-D-arabino-heptulosonate 7-phosphate synthase (Fig. 7). By catalyzing the production of erythrose-4-phosphate, transketolase (TK) mediates phenylpropanoid metabolism. In particular, a decrease in chloroplastic TK activity results in the decreased abundance of precursors for lignin synthesis [72]. Similarly, inhibition of enolase activity, which converts 2-phosphoglycerate into phosphoenolpyruvate, strongly limits secondary pathways such as the shikimate branch of amino acid biosynthesis [73]. Relative to the woody stem part, the upper stem segments have a significantly higher abundance of chloroplast TK (spots 416, 430, 444 and 445) and a higher abundance of enolase (spot 921) (Fig. 5H). With respect to their implication in phenylpropanoid metabolism, the differential accumulation of these proteins supports the idea that the synthesis of lignin precursors is more active in the two upper stem regions in comparison to the mature basal part. This correlates with the stabilization of the proportions of lignin and with the stagnation of the proportion of intrafascicular xylem *per* vascular bundle down from the intermediate stem part (Figs. S1D and S2)

4.3.3. Mitochondrial respiration

Besides being used in the sucrose pathway and secondary metabolism, 3PGA is converted into pyruvate during the last step of glycolysis (Fig. 7). Following the pyruvate dehydrogenase reaction, pyruvate is converted into acetyl-CoA and enters the TCA cycle. The conversion of pyruvate into acetyl-CoA involves the pyruvate

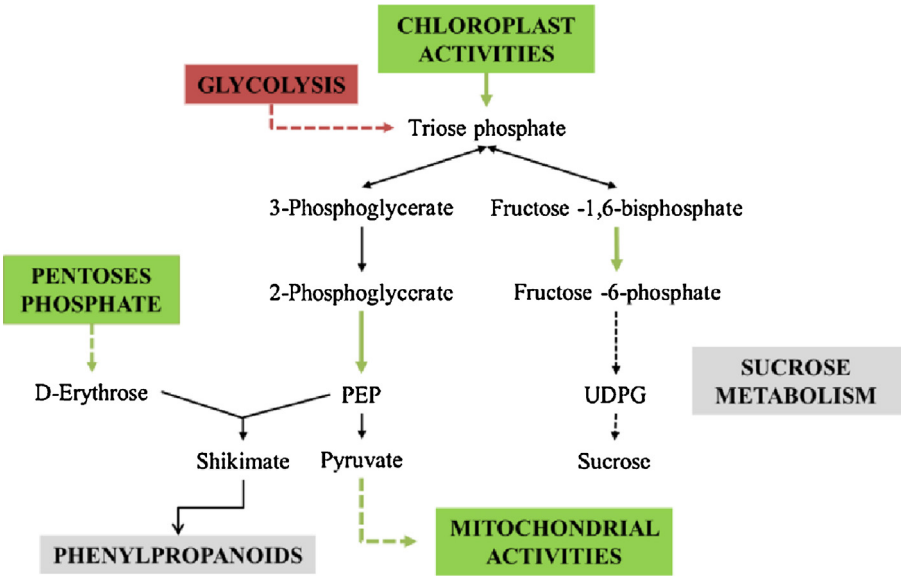

Fig. 7. Evolution of the main cytosolic routes which are differentially regulated between apical (1/5) and basal (5/5) region. Green boxes/arrows and red boxes/arrows indicate, respectively, biological routes in which proteins are of higher and lower abundance in the apex.

dehydrogenase complex. In the two youngest regions, two spots containing pyruvate dehydrogenase E1 component subunit beta (spot 1384) and mitochondrial aldehyde dehydrogenase family 2 member B4 (spot 2983) are increased in abundance in comparison with the basal stem segment (Fig. 5I). The simultaneous increase in abundance of proteins directly involved in mitochondrial activities (NADH:ubiquinone oxidoreductase (spot 388), and ATPase alpha F1 (spot 805) confirms the higher energetic needs of the growing regions of the stems where fibre maturation occurs.

4.4. Forisome proteins accumulate in the most mature stem regions

Mature sieve elements are connected to each other at the sieve plate perforated by numerous pores assuring a symplastic continuity of the sieve tubes. In *Fabaceae*, typical crystalline phloem-specific proteins (forisomes) have been demonstrated to undergo rapid conformational changes, from a condensed to a dispersed state in response to variations in Ca^{2+} concentration [74,75]. In their dispersed form, these forisomes have been proposed to form plugs able to modulate the phloem flux [74]. This latter suggestion has recently gained in plausibility by using artificial sieve elements models [76]. Forisomes already appear in immature sieve elements in the form of small thin crystalline structures which develop a tail when sieve tubes differentiate. They remain but fray out into filaments and striated fibrils in mature sieve elements [77]. Molecular characterization of the forisome component For1 indicated a strict expression of *for1* genes in immature sieve elements, concomitantly with a higher activity of the *for1* promoter. In particular, *for1* promoter activity was detected in the stem at sites where secondary growth occurs [78]. In this study, the gradual increase in thickness of the vascular bundle revealed by microscopic imaging (Fig. 1) is associated with a significant accumulation of sieve element occlusion 3 (SEO3) proteins from the apex to the base of the stem (spot 428) (Table S2).

4.5. Typical basal proteins: redox regulation and stress-related proteins

Finally, one major characteristic of the basal regions of the stem is the accumulation of oxidative stress-related and stress-responsive proteins. Among these, peroxisomal membrane proteins (spot 1339), monodehydroascorbate reductase (spot 1215) and flavoproteins wrbA-like (spots 2019 and 2020) are more accumulated in these mature regions as compared with the apical part (Table S2 and Fig. 5J). Similarly, Pprg2 (spots 2543) member of the PR-10 family and harvest-induced proteins (spot 2576) display the highest fold-changes in this study (Table S2 and Fig. 5J). They have a ligand-binding bet_v_1 domain susceptible to respond to hormonal stimuli such as ABA [79]. In alfalfa, the higher expression of RNA coding for homologous proteins has been reported following drying, heat stress or direct freezing [79]. Furthermore, Pprg2 proteins have been described in the roots of *M. truncatula* responding to auxin treatment, to *Sinorhizobium meliloti* inoculation [80], in stem region of alfalfa parasitized by dodder and may be involved in the general plant response to bacterial infection [81]. We noticed a strong anti-correlation between the abundance of these stress-responsive proteins and that of fructose-1,6-bisphosphatase in spot 1332, the fructose bisphosphate aldolase in spot 1316 and cpn60 in spot 701 (Table 2). In fact, these Pprg2 proteins accumulate in the stem region where almost all proteins involved in photosynthesis and respiration were of lower abundance, which suggests

Table 2
Correlation coefficient observed between proteins from the ligand-binding bet_v_1 domain family and the other differentially expressed proteins (represented are the proteins having at least one coefficient inferior to −0.90 or superior to 0.90).

		TCP-1/cpn60 chaperonin family protein Spot 701	Fructose bisphosphate aldolase Spot 1316	Fructose-1,6-bisphosphatase Spot 1332	Pprg2 protein Spot 2543	Harvest-induced protein Spot 2576
Spot 2543	Pprg2 protein	**−0.92**	**−0.92**	**−0.95**	1.00	**0.95**
Spot 2576	harvest-induced protein	−0.86	**−0.93**	−0.86	**0.95**	1.00

that their regulation may be linked to the normal developmental process rather than to an external parasitic induction. Among the other proteins which accumulate in the fibrous basal region are secreted proteins affected by biotic stress tolerance, such as a multifaceted apoplast endochitinase (spot 1415) involved in both development and pathogenic plant response and a TolB protein (spot 2586) already observed to increase in abundance following pathogen infection in *A. thaliana* [82].

5. Conclusions

Our data highlight a metabolic switch occurring along the stem of alfalfa. From the establishment of the photosynthetic machinery in the apical part to the accumulation of redox and stress-related proteins in the most basal segment, each stem region develops its own proteome profile. The high abundance of proteins involved in chloroplast and mitochondrial activities coincides with an increase in the proportions of the different fibres and with a higher expression of genes coding for cellulose synthases putatively regulating secondary wall biogenesis. This suggests that the photosynthetic metabolism of the stem provides at least partially the basic building blocks for the production of the fibrous material. Far from being metabolically inactive, the mature stem regions accumulate proteins commonly observed in response to biotic/abiotic stresses. Since the base of the stem is in the direct vicinity to the ground ecosystem, the higher accumulation of stress-related proteins may be associated with the acquisition of functions linked with plant defence, thus protecting the plant against external aggressions.

Acknowledgments

We kindly acknowledge Lucien Hoffmann for careful reading, Laurent Solinhac for his precious help, Céline Leclercq and Sébastien Planchon for their support during the proteomics experiments.

Appendix A. Supplementary data

Supplementary data associated with this article can be found, in the online version, at http://dx.doi.org/10.1016/j.plantsci.2015.05.014

References

[1] A. Elo, J. Immanen, K. Nieminen, Y. Helariutta, Stem cell function during plant vascular development, Semin. Cell. Dev. Biol. 20 (2009) 1097–1106.
[2] J.P. Matte Risopatron, Y. Sun, B.J. Jones, The vascular cambium: molecular control of cellular structure, Protoplasma 247 (2010) 145–161.
[3] L.E. Sieburth, M.K. Deyholos, Vascular development: the long and winding road, Curr. Opin. Plant Biol. 9 (2006) 48–54.
[4] B. Sattelmacher, The apoplast and its significance for plant mineral nutrition, New Phytol. 149 (2001) 167–192.
[5] D.J. Cosgrove, Wall structure and wall loosening: a look backwards and forwards, Plant Physiol. 125 (2001) 131–134.
[6] A. Sampathkumar, L. Neumetzler, S. Persson, The plasma membrane and the cell wall, in: A.S. Murphy, B. Schulz, W. Peer (Eds.), The Plant Plasma Membrane, Springer, Berlin, Heidelberg, 2011, pp. 57–85.
[7] C. Ellis, I. Karafyllidis, C. Wasternack, J.G. Turner, The Arabidopsis mutant cev1 links cell wall signaling to jasmonate and ethylene responses, Plant Cell 14 (2002) 1557–1566.
[8] C. Vallet, G. Lemaire, B. Monties, B. Chabbert, Cell wall fractionation of alfalfa stem in relation to internode development: biochemistry aspect, J. Agric. Food Chem. 46 (1998) 3458–3467.
[9] F.M.J.H.G. Engels, Alfalfa stem tissues: cell-wall development and lignification, Ann. Bot. 82 (1998) 561–568.
[10] S. Kumar, Biotechnological advancements in alfalfa improvement, J. Appl. Genet. 52 (2011) 111–124.
[11] M.S.S. Reddy, F. Chen, G. Shadle, L. Jackson, H. Aljoe, R.A. Dixon, Targeted down-regulation of cytochrome P450 enzymes for forage quality improvement in alfalfa (*Medicago sativa* L.), Proc. Natl. Acad. Sci. USA 102 (2005) 16573–16578.
[12] H.J. Jung, D.A. Samac, G. Sarath, Modifying crops to increase cell wall digestibility, Plant Sci. 185–186 (2012) 65–77.
[13] S.S. Yang, W.W. Xu, M. Tesfaye, J.F. Lamb, H.J. Jung, K.A. VandenBosch, C.P. Vance, J.W. Gronwald, Transcript profiling of two alfalfa genotypes with contrasting cell wall composition in stems using a cross-species platform: optimizing analysis by masking biased probes, BMC Genomics 11 (2010) 323.
[14] P.J. Van Soest, J.B. Robertson, B.A. Lewis, Methods for dietary fiber, neutral detergent fiber, and nonstarch polysaccharides in relation to animal nutrition, J. Dairy Sci. 7 (4) (1991) 3583–3597.
[15] J. Stuth, A. Jama, D. Tolleson, Direct and indirect means of predicting forage quality through near infrared reflectance spectroscopy, Field Crop Res. 84 (2003) 45–56.
[16] R. Vanholme, B. Demedts, K. Morreel, J. Ralph, W. Boerjan, Lignin biosynthesis and structure, Plant Phys. 153 (2010) 895–905.
[17] R. Vanholme, K. Morreel, C. Darrah, P. Oyarce, J.H. Grabber, J. Ralph, W. Boerjan, Metabolic engineering of novel lignin in biomass crops, New Phytol. 196 (2012) 978–1000.
[18] Y. Wang, M. Chantreau, R. Sibout, S. Hawkins, Plant cell wall lignification and monolignol metabolism, Front. Plant Sci. 4 (2013), 220.
[19] S. Fujii, T. Hayashi, K. Mizuno, Sucrose synthase is an integral component of the cellulose synthesis machinery, Plant Cell Physiol. 51 (2010) 294–301.
[20] A.R. Paredez, C.R. Somerville, D.W. Ehrhardt, Visualization of cellulose synthase demonstrates functional association with microtubules, Science 312 (2006) 1491–1495.
[21] E.F. Crowell, V. Bischoff, T. Desprez, A. Rolland, Y.D. Stierhof, K. Schumacher, M. Gonneau, H. Höfte, S. Vernhettes, Pausing of golgi bodies on microtubules regulates secretion of cellulose synthase complexes in *Arabidopsis*, Plant Cell 21 (2009) 1141–1154.
[22] R. Wightman, S. Turner, Trafficking of the plant cellulose synthase complex, Plant Physiol. 153 (2010) 427–432.
[23] G. Guerriero, K. Sergeant, J.F. Hausman, Wood biosynthesis and typologies: a molecular rhapsody, Tree Physiol. 38 (2014) 839–855.
[24] S.J. Lee, R.S. Saravanan, C.M. Damasceno, H. Yamane, B.D. Kim, J.K. Rose, Digging deeper into the plant cell wall proteome, Plant Physiol. Biochem. 42 (2004) 979–988.
[25] E. Jamet, H. Canut, G. Boudart, R.F. Pont-Lezica, Cell wall proteins: a new insight through proteomics, Trends Plant Sci. 11 (2006) 33–39.
[26] T.A. Gorshkova, V.V. Sal'nikova, S.B. Chemikosova, M.V. Ageeva, N.V. Pavlencheva, J.E.G. van Dam, The snap point: a transition point in *Linum usitatissimum* bast fiber development, Ind. Crops Prod. 18 (2003) 213–221.
[27] A. Day, K. Ruel, G. Neutelings, D. Cronier, H. David, S. Hawkins, B. Chabbert, Lignification in the flax stem: evidence for an unusual lignin in bast fibers, Planta 222 (2005) 234–245.
[28] N. Hotte, M. Deyholos, A flax fibre proteome: identification of proteins enriched in bast fibres, BMC Plant Biol. 8 (2008) 52.
[29] M. Schuetz, R. Smith, B. Ellis, Xylem tissue specification, patterning, and differentiation mechanisms, J. Exp. Bot. 6 (4) (2013) 11–31.
[30] D. Tolivia, J. Tolivia, Fasga, A new polychromatic method for simultaneous and differential staining of plant tissues, J. Microsc. 148 (1987) 113–117.
[31] M.M. Bradford, A rapid and sensitive method for the quantitation of microgram quantities of protein utilizing the principle of protein-dye binding, Anal. Biochem. 72 (1976) 248–254.
[32] B. Printz, K. Sergeant, S. Lutts, C. Guignard, J. Renaut, J.F. Hausman, From tolerance to acute metabolic deregulation: contribution of proteomics to dig into the molecular response of alder-species under a polymetallic exposure, J. Prot. Res. 12 (2013) 5160–5179.
[33] G. Guerriero, S. Legay, J.F. Hausman, Alfalfa cellulose synthase gene expression under abiotic stress: a hitchhiker's guide to RT-qPCR normalization, PLoS ONE 9 (2014) e103808.
[34] J. Vandesompele, K. De Preter, F. Pattyn, B. Poppe, N. Van Roy, A. De Paepe, F. Speleman, Accurate normalization of real-time quantitative RT-PCR data by geometric averaging of multiple internal control genes, Genome Biol. 3 (2002), research00034.
[35] S.S. Yang, Z.J. Tu, F. Cheung, W.W. Xu, J.F. Lamb, H.J. Jung, C.P. Vance, J.W. Gronwald, Using RNA-Seq for gene identification, polymorphism detection and transcript profiling in two alfalfa genotypes with divergent cell wall composition in stems, BMC Genomics 12 (2011) 199.
[36] J. Hellemans, G. Mortier, A. De Paepe, F. Speleman, J. Vandesompele, qBase relative quantification framework and software for management and automated analysis of real-time quantitative PCR data, Genome Biol. 8 (2007) R19.
[37] M.B. Eisen, P.T. Spellman, P.O. Brown, D. Botstein, Cluster analysis and display of genome-wide expression patterns, Proc. Natl. Acad. Sci. USA 95 (1998) 14863–14868.
[38] A.J. Saldanha, Java Treeview—extensible visualization of microarray data, Bioinformatics 20 (2004) 3246–3248.
[39] P. Teppola, Near-infrared spectroscopy. Principles, instruments, applications, J. Chemometrics 16 (2002) 636–638.
[40] J.P. Conzen, Multivariate Calibration, A Practical Guide for Developing Methods in the Quantitative Analytical Chemistry, Ettlingen, Germany, 2006.
[41] E.T. Nilsen, The influence of water stress on leaf and stem photosynthesis in *Spartium junceum* L, Plant Cell Environ. 15 (1992) 455–461.
[42] E.T. Nilsen, M.R. Sharifi, Seasonal acclimation of stem photosynthesis in woody legume species from the Mojave and Sonoran Deserts of California, Plant Physiol. 105 (1994) 1385–1391.
[43] P.A. Shirke, Leaf photosynthesis, dark respiration and fluorescence as influenced by leaf age in an evergreen tree *Prosopis juliflora*, Photosynthetica 39 (2001) 305–311.

[44] M.S. Doblin, I. Kurek, D. Jacob-Wilk, D.P. Delmer, Cellulose biosynthesis in plants: from genes to rosettes, Plant Cell Physiol. 43 (2002) 1407–1420.
[45] G. Guerriero, J. Fugelstad, V. Bulone, What do we really know about cellulose biosynthesis in higher plants? J. Integr. Plant Biol. 52 (2010) 161–175.
[46] D.J. Cosgrove, Growth of the plant cell wall, Nat. Rev. Mol. Cell Biol. 6 (2005) 850–861.
[47] S. Persson, A. Paredez, A. Carroll, H. Palsdottir, M. Doblin, P. Poindexter, N. Khitrov, M. Auer, C.R. Somerville, Genetic evidence for three unique components in primary cell-wall cellulose synthase complexes in *Arabidopsis*, Proc. Natl. Acad. Sci. USA 104 (2007) 15566–15571.
[48] I.I. Atanassov, J.K. Pittman, S.R. Turner, Elucidating the mechanisms of assembly and subunit interaction of the cellulose synthase complex of *Arabidopsis* secondary cell walls, J. Biol. Chem. 284 (2009) 3833–3841.
[49] A. Carroll, N. Mansoori, S. Li, L. Lei, S. Vernhettes, R.G. Visser, C. Somerville, Y. Gu, L.M. Trindade, Complexes with mixed primary and secondary cellulose synthases are functional in *Arabidopsis* plants, Plant Physiol. 160 (2012) 726–737.
[50] S. Li, L. Lei, Y. Gu, Functional analysis of complexes with mixed primary and secondary cellulose synthases, Plant Signal. Behav. 8 (2013) e23179.
[51] A. Hafrén, K. Eskelin, K. Mäkinen, Ribosomal protein P0 promotes potato virus A infection and functions in viral translation together with VPg and eIF(iso)4E, J. Virol. 87 (2013) 4302–4312.
[52] M. Bar-Peled, M.A. O'Neill, Plant nucleotide sugar formation, interconversion, and salvage by sugar recycling, Annu. Rev. Plant. Biol. 6 (2) (2011) 127–155.
[53] M.B. Ali, S. Khatun, E.J. Hahn, K.Y. Paek, Enhancement of phenylpropanoid enzymes and lignin in *Phalaenopsis* orchid and their influence on plant acclimatisation at different levels of photosynthetic photon flux, Plant Growth Regul. 49 (2006) 137–146.
[54] Q. Wang, R.W. Sullivan, A. Kight, R.L. Henry, J. Huang, A.M. Jones, K.L. Korth, Deletion of the chloroplast-localized Thylakoid Formation1 gene product in *Arabidopsis* leads to deficient thylakoid formation and variegated leaves, Plant Physiol. 1 (36) (2004) 3594–3604.
[55] L. Zhang, Y. Kato, S. Otters, U.C. Vothknecht, W. Sakamoto, Essential role of VIPP1 in chloroplast envelope maintenance in *Arabidopsis*, Plant Cell 24 (2012) 3695–3707.
[56] D. von Wettstein, S. Gough, C.G. Kannangara, Chlorophyll biosynthesis, Plant Cell 7 (1995) 1039–1057.
[57] D. Aarti, R. Tanaka, H. Ito, A. Tanaka, High light inhibits chlorophyll biosynthesis at the level of 5-aminolevulinate synthesis during de-etiolation in cucumber (*Cucumis sativus*) cotyledons, Photochem. Photobiol. 83 (2007) 171–176.
[58] J. Andersson, M. Wentworth, R.G. Walters, C.A. Howard, A.V. Ruban, P. Horton, S. Jansson, Absence of the Lhcb1 and Lhcb2 proteins of the light-harvesting complex of photosystem II—effects on photosynthesis, grana stacking and fitness, Plant J. 35 (2003) 350–361.
[59] S. Caffarri, R. Kouril, S. Kereïche, E.J. Boekema, R. Croce, Functional architecture of higher plant photosystem II supercomplexes, EMBO J. 28 (2009) 3052–3063.
[60] R. Croce, H. van Amerongen, Light-harvesting and structural organization of Photosystem II: from individual complexes to thylakoid membrane, J. Photochem. Photobiol. B 104 (2011) 142–153.
[61] N. Carrillo, E.A. Ceccarelli, Open questions in ferredoxin-NADP+ reductase catalytic mechanism, Eur. J. Biochem. 270 (2003) 1900–1915.
[62] A.U. Igamberdiev, M.R. Roussel, Feedforward non-Michaelis–Menten mechanism for CO_2 uptake by Rubisco: contribution of carbonic anhydrases and photorespiration to optimization of photosynthetic carbon assimilation, Biosystems 107 (2012) 158–166.
[63] M. Broin, S. Cuiné, F. Eymery, P. Rey, The plastidic 2-cysteine peroxiredoxin is a target for a thioredoxin involved in the protection of the photosynthetic apparatus against oxidative damage, Plant Cell 14 (2002) 1417–1432.
[64] G. Aschan, H. Pfanz, Non-foliar photosynthesis—a strategy of additional carbon acquisition, Flora 198 (2003) 81–97.
[65] E.A.H. Avila, W. Tezara, Contribution of stem CO_2 fixation to whole-plant carbon balance in nonsucculent species, Photosynthetica 52 (2014) 3–15.
[66] A. Strand, R. Zrenner, S. Trevanion, M. Stitt, P. Gustafsson, P. Gardeström, Decreased expression of two key enzymes in the sucrose biosynthesis pathway, cytosolic fructose-1,6-bisphosphatase and sucrose phosphate synthase, has remarkably different consequences for photosynthetic carbon metabolism in transgenic *Arabidopsis thaliana*, Plant J. 23 (2000) 759–770.
[67] S.K. Lee, J.S. Jeon, F. Börnke, L. Voll, J.I. Cho, C.H. Goh, S.W. Jeong, Y.I. Park, S.J. Kim, S.B. Choi, A. Miyao, H. Hirochika, G. An, M.H. Cho, S.H. Bhoo, U. Sonnewald, T.R. Hahn, Loss of cytosolic fructose-1,6-bisphosphatase limits photosynthetic sucrose synthesis and causes severe growth retardations in rice (*Oryza sativa*), Plant Cell Environ. 31 (2008) 1851–1863.
[68] M.H. Cho, A. Jang, S.H. Bhoo, J.S. Jeon, T.R. Hahn, Manipulation of triose phosphate/phosphate translocator and cytosolic fructose-1,6-bisphosphatase, the key components in photosynthetic sucrose synthesis, enhances the source capacity of transgenic *Arabidopsis* plants, Photosynth. Res. 111 (2012) 261–268.
[69] X. Chen, N.G. Irani, J. Friml, Clathrin-mediated endocytosis: the gateway into plant cells, Curr. Opin. Plant Biol. 14 (2011) 674–682.
[70] L. Bashline, S. Li, C.T. Anderson, L. Lei, Y. Gu, The endocytosis of cellulose synthase in Arabidopsis is dependent on m2, a clathrin-mediated endocytosis adaptin, Plant Physiol. 163 (2013) 150–160.
[71] C.T. Simons, A. Staes, H. Rommelaere, C. Ampe, S.A. Lewis, N.J. Cowan, Selective contribution of eukaryotic prefoldin subunits to actin and tubulin binding, J. Biol. Chem. 279 (2004) 4196–4203.
[72] S. Henkes, U. Sonnewald, R. Badur, R. Flachmann, M. Stitt, A small decrease of plastid transketolase activity in antisense tobacco transformants has dramatic effects on photosynthesis and phenylpropanoid metabolism, Plant Cell 13 (2001) 535–551.
[73] L.M. Voll, M.R. Hajirezaei, C. Czogalla-Peter, W. Lein, M. Stitt, U. Sonnewald, F. Börnke, Antisense inhibition of enolase strongly limits the metabolism of aromatic amino acids, but has only minor effects on respiration in leaves of transgenic tobacco plants, New Phytol. 184 (2009) 607–618.
[74] M. Knoblauch, W.S. Peters, K. Ehlers, A.J. van Bel, Reversible calcium-regulated stopcocks in legume sieve tubes, Plant Cell 13 (2001) 1221–1230.
[75] M. Knoblauch, W.S. Peters, Forisomes, a novel type of Ca^{2+}-dependent contractile protein motor, Cell Motil. Cytoskeleton 58 (2004) 137–142.
[76] M. Knoblauch, M. Stubenrauch, A.J. van Bel, W.S. Peters, Forisome performance in artificial sieve tubes, Plant Cell Environ. 35 (2012) 1419–1427.
[77] B.A. Palevitz, E.H. Newcomb, The ultrastructure and development of tubular and crystalline P-protein in the sieve elements of certain papilionaceous legumes, Protoplasma 72 (1971) 399–426.
[78] G.A. Noll, M.E. Fontanellaz, B. Rüping, A. Ashoub, A.J. van Bel, R. Fischer, M. Knoblauch, D. Prüfer, Spatial and temporal regulation of the forisome gene for1 in the phloem during plant development, Plant Mol. Biol. 65 (2007) 285–294.
[79] J. Zhang, W.J. Yu, A.S. Xiong, B. Bahramnejad, L.R. Erickson, Isolation and characterization of a harvest-induced promoter of an alfalfa gene, hi7, Plant Growth Regul. 64 (2011) 119–128.
[80] G.E. van Noorden, T. Kerim, N. Goffard, R. Wiblin, F.I. Pellerone, B.G. Rolfe, U. Mathesius, Overlap of proteome changes in *Medicago truncatula* in response to auxin and *Sinorhizobium meliloti*, Plant Physiol. 144 (2007) 1115–1131.
[81] T. Borsics, M. Lados, Dodder infection induces the expression of a pathogenesis-related gene of the family PR-10 in alfalfa, J. Exp. Bot. 53 (2002) 1831–1832.
[82] C. Holzmeister, A. Fröhlich, H. Sarioglu, N. Bauer, J. Durner, C. Lindermayr, Proteomic analysis of defense response of wildtype *Arabidopsis thaliana* and plants with impaired NO- homeostasis, Proteomics 11 (2011) 1664–1683.